Critical grid size for simulating convective storms: A case study of the Del City supercell storm

A. Noda and H. Niino

Ocean Research Institute, The University of Tokyo, Tokyo, Japan

Received 7 April 2003; revised 6 July 2003; accepted 23 July 2003; published 21 August 2003.

[1] The dependence of a numerically-simulated 'Del City' supercell storm on grid size is studied. A reference run with the grid size of 0.5 km successfully reproduces the supercell as demonstrated in the previous studies. In this sensitivity study, the grid size is varied from 1.0 km to 3.0 km with an interval of 100 m. When the grid size is less than 2.5 km, the storm evolves in a manner qualitatively similar to the reference run. When it is larger than 2.5 km, however, the evolution of the storm changes drastically because of an insufficient estimation of the shear-induced dynamic pressure. The present "critical grid size" is much smaller than that expected from the former sensitivity studies. Thus, one has to be more careful in choosing the grid size when performing a prediction of mesoscale convective systems, the behavior of which depends strongly on the behavior of individual meso-γ-scale convective storms. *INDEX TERMS:* 3314 Meteorology and Atmospheric Dynamics: Convective processes; 3329 Meteorology and Atmospheric Dynamics: Mesoscale meteorology; 3337 Meteorology and Atmospheric Dynamics: Numerical modeling and data assimilation. **Citation:** Noda, A., and H. Niino, Critical grid size for simulating convective storms: A case study of the Del City supercell storm, *Geophys. Res. Lett.*, *30*(16), 1844, doi:10.1029/2003GL017498, 2003.

1. Introduction

[2] Progress in computer technology now allows us to simulate meso-α- or meso-β-scale precipitation systems with a horizontal grid spacing of 2–5 km [e.g., *Kato*, 1996; *Yanase et al.*, 2002]. In such simulations, meso-γ-scale convective storms which develop in the meso-α- or β-scale precipitation system are often assumed to be resolved explicitly, so that no cumulus parameterization is used. However, to what extent a numerical model with $2 \sim 5$ km grid size reproduces realistically the behaviors of convective storms is not obvious. If individual convective storms were not reproduced realistically, it would not be hoped that the meso-α- or β-scale systems are predicted satisfactorily. To answer this problem, it seems necessary to clarify how the variation of the grid size affects the simulated individual convective storms.

[3] There have been only few studies which attempted to investigate the sensitivity of a simulated convective storm on the grid size. *Weisman et al.* [1997] suggested that the grid size of 4 km is sufficient to reproduce the characteristics of a simulated squall line. Recently, *Adlerman and Droegemeier* [2002] examined this problem for a supercell storm, which develops in an environment with a strong shear and often produces severe weather such as tornadoes and hail. They have found that the cyclic generation of the mesocyclone is significantly affected by the model resolution.

[4] In this study, we focus on the Del City supercell storm which took place in central Oklahoma on 20 May 1977, since its basic behavior is relatively well known [e.g., *Klemp and Wilhelmson*, 1978; *Adlerman et al.*, 1999; *Adlerman and Droegemeier*, 2002]. We will demonstrate that the evolution of the storm such as a storm splitting can depend on grid resolution significantly.

2. Numerical Model

[5] The numerical model used for the present simulation is ARPS Version 4.5.1 [*Xue et al.*, 1995]. In order to examine the sensitivity of the simulated convective storm to the horizontal resolution of the model, we have performed 21 experiments in which the horizontal grid size is varied from 1.0 km to 3.0 km with 0.1 km interval. Hereafter, an experiment with a horizontal grid size of x km is referred to as the x km-run.

[6] To make sure that the sensitivity solely to the horizontal grid size is examined, all the other conditions are kept the same. The size of the calculation domain is 127 km $\times$ 127 km in the horizontal directions and 16.3 km in the vertical direction. Vertical grid size varies from 100 m near the ground to 600 m near the model top.

[7] Free-slip and adiabatic conditions are assumed at the top and bottom boundaries. Radiation conditions are assumed at the lateral open boundaries. Rayleigh damping with the e-folding time of 300 s is introduced above z = 12 km. Only the Kessler-type warm rain process is considered in the cloud physics. The turbulent mixing is expressed by the 1.5-order closure scheme. A 4th-order computational mixing proportional to the 4th power of the grid size with a coefficient of 5×10^{-4} s^{-1} is employed. The Coriolis force is not included.

[8] The vertical sounding data for the Del City supercell is given as the horizontally uniform initial condition as in *Klemp and Wilhelmson* [1978]. In order to initiate the storm, an ellipsoidal thermal bubble with horizontal and vertical radii of 10 km and 1.5 km, respectively, is placed at z = 1.5 km at the center of the calculation domain. The maximum temperature anomaly of the bubble is 4 K. In order to keep the storm in the calculation domain, the model coordinate system is translated eastward at 3.0 m s^{-1} and northward at 14.0 m s^{-1}. All the physical values hereafter shown are storm-relative.

3. Results

3.1. Reference Run

[9] As is shown in the previous studies [*Adlerman et al.*, 1999; *Adlerman and Droegemeier*, 2002], the grid size of

0094-8276/03/2003GL017498

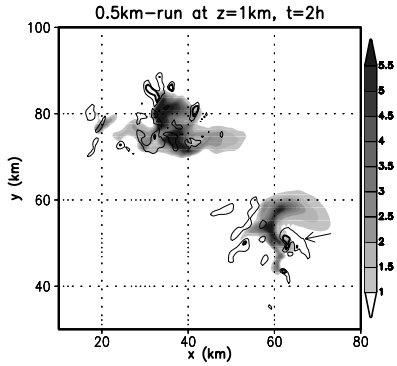

Figure 1. Horizontal distribution of rain water and vertical vorticity for the 0.5 km-run at $z = 1$ km for $t = 2$h. The gray scale shows the rain water distribution in g kg^{-1}. The thin and thick contour lines indicate the vertical vorticity of 0.3×10^{-2} s^{-1} and 1.0×10^{-2} s^{-1}, respectively. The arrow points to the mesocyclone.

0.5 km is fine enough to reproduce the basic characteristics of the Del City supercell. Therefore, we take the 0.5 km-run as the reference run to be compared with other experiments.

[10] Figure 1 shows the horizontal cross section of rain water and vertical vorticity fields at $z = 1$ km for $t = 2$h for the 0.5-km run. The initial storm splits into left- and right-movers, and the right-mover intensifies much more than the left-mover does. A region of intense vertical vorticity called a mesocyclone develops in the right-mover. The intense cyclonic circulation in the mesocyclone produces the hook-shaped rain water pattern.

3.2. Experiments With Different Grid Sizes

[11] Figure 2 shows horizontal cross sections of rain water and vertical vorticity fields for the 2.1 km-run–2.9 km-run at $z = 1$ km for $t = 2$h. It is found that after splitting, the right-mover for the grid size of less than 2.5 km shows supercellular characteristics such as a region of positive vertical vorticity and an associated hook-shaped rain water distribution (cf. Figure 1). When the grid size is increased to 2.6 km, however, the evolution of the split storms change drastically. The right-mover, which intensifies for the finer resolutions, starts to weaken significantly while the left-mover weakens little. When the grid size is larger than 2.8 km, even the left-mover is not maintained and dissipates.

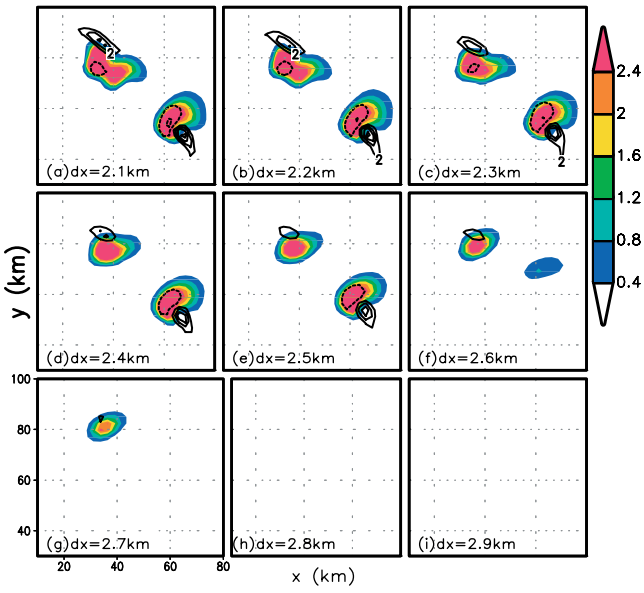

Figure 2. Horizontal distributions of rain water (shaded; g kg^{-1}) and vertical vorticity (contour line for every 1×10^{-3} s^{-1} interval with 0 m s^{-1} line omitted) at $z = 1$ km for $t = 2$h for the 2.1 km-run–2.9 km-run. The solid and broken lines denote positive and negative values, respectively. Only a part of the calculation domain is shown.

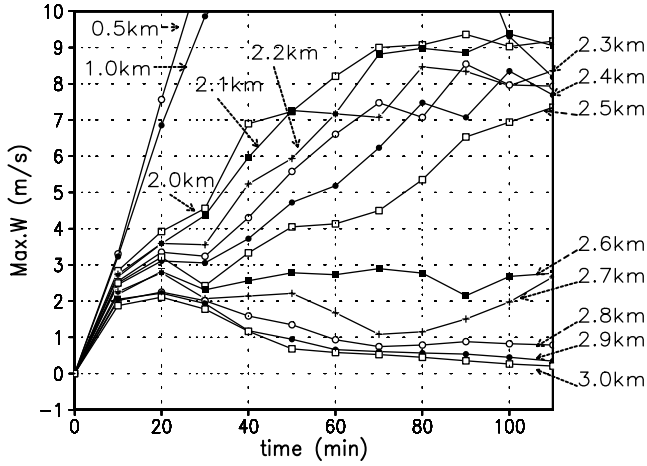

Figure 3. Time-evolutions of the maximum vertical velocities in the whole horizontal domain at $z = 1$ km for the 0.5 km-run–3.0 km-run.

[12] Figure 3 shows the time evolutions of the maximum updraft of the storms in the whole horizontal domain at $z = 1$ km for the various runs with different horizontal resolutions. For the 0.5 km- and 1.0 km-runs, the updraft develops much more rapidly and attains larger values. Although the updraft for the 2.0 km-run is much weaker than that for the 0.5 km- and 1.0 km-runs, the right-mover clearly exhibits supercellular characteristics (cf. Figure 2). As the grid size is increased, the intensity of the updraft tends to decrease. This tendency agrees with the case of the simulated squall lines studied by *Weisman et al.* [1997]. We note a significant gap between the lines for the 2.5 km and 2.6 km-runs, corresponding to the qualitative change in the evolution of the split storms (see Figure 2).

3.3. Comparison Between the 2.5 km- and 2.6 km-runs

[13] In this section, we will focus on the difference in the behavior of the right-movers between the 2.5 km- and 2.6 km-runs and examine the reason why the storm fails to evolve into a supercell in the latter.

[14] Figure 4 shows a close-up view of the horizontal distributions of rain water and vertical velocity fields for the 2.5 km- and 2.6 km-runs at $z = 1$ km at $t = 40$ min when the updraft for both runs starts to show different magnitudes. It is seen that, for both runs, an updraft of about 3 m s^{-1} which is accompanied by positive vertical vorticity (cf. Figure 2) is present in the southeast part of the right-mover. Such a 'rotating updraft', though its vorticity does not reach the criterion of a mesocyclone ($\geq$0.01 s^{-1}), is characteristic of the supercell. The updraft and downdraft for the 2.6 km-run, however, are already somewhat weaker than those for the 2.5 km-run.

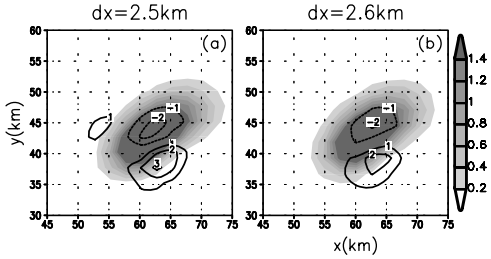

Figure 4. Horizontal distributions of rain water (shaded; g kg^{-1}) and vertical velocity (contour line for every 1 m s^{-1} with 0 m s^{-1} line omitted) at z = 1 km at t = 40 min for the (a) 2.5 km- and (b) 2.6 km-runs.

[15] In order to examine the cause why the updrafts in the right-movers for the 2.5 km-run and the 2.6 km-run start to show remarkable difference in their evolutions, we follow *Rotunno and Klemp* [1982] to examine the pressure perturbation (π) by decomposing it into linear (π_L), nonlinear (π_{NL}) and buoyancy (π_B) terms: The momentum equation in the vertical direction can be written as

$$\frac{\partial w}{\partial t} = -\boldsymbol{v}\cdot\nabla w - C_p\Theta\frac{\partial \pi}{\partial z} + B$$

$$= \underbrace{-\boldsymbol{v}\cdot\nabla w}_{F_A} \underbrace{-C_p\Theta\frac{\partial \pi_L}{\partial z}}_{F_L} \underbrace{-C_p\Theta\frac{\partial \pi_{NL}}{\partial z}}_{F_{NL}} \underbrace{-C_p\Theta\frac{\partial \pi_B}{\partial z} + B}_{F_B}, \qquad (1)$$

where π denotes the Exner function, B the buoyancy, C_p (= 1004 J K^{-1}) the specific heat of dry air at constant pressure, Θ(=300 K) standard potential temperature. The right-hand side of Equation (1) is grouped into four parts: F_A is the advection term, F_L and F_{NL} are forcing terms relating to π_L and π_{NL}, respectively, and F_B the buoyancy, where the pressure perturbations π_L, π_{NL} and π_B are obtained by solving the following Poisson equations:

$$\nabla^2\pi_L = -\frac{2}{C_p\Theta}\left(\frac{\partial \bar{u}}{\partial z}\frac{\partial w}{\partial x} + \frac{\partial \bar{v}}{\partial z}\frac{\partial w}{\partial y}\right), \qquad (2)$$

$$\nabla^2\pi_{NL} = -\frac{1}{C_p\Theta}\left[\left(\frac{\partial u}{\partial x}\right)^2 + \left(\frac{\partial v}{\partial y}\right)^2 + \left(\frac{\partial w}{\partial z}\right)^2 + 2\left(\frac{\partial u'}{\partial z}\frac{\partial w}{\partial x} + \frac{\partial v'}{\partial z}\frac{\partial w}{\partial y} + \frac{\partial v}{\partial x}\frac{\partial u}{\partial y}\right)\right], \qquad (3)$$

$$\nabla^2\pi_b = \frac{g}{C_p\Theta}\frac{\partial B}{\partial z}. \qquad (4)$$

The overbar and prime denote a quantity of the basic state and a deviation from it, respectively. For solving the Poisson equations, a no-gradient condition is used for lateral boundaries. For top and bottom boundaries, a hydrostatic condition is used for π_B, while no-gradient conditions for π_L and π_{NL}.

[16] Figure 5 displays horizontal distributions of the right-hand side of Equation (1) at z = 1 km for the 2.5 km- and 2.6 km-runs. First, let us look at the results for the 2.5 km-run (Figure 5a–5e). F_A is negative in the eastern side of the updraft region (Figure 5b). F_B is also mostly negative (Figure 5c). This is because z = 1 km is below the level of free convection, suggesting that the upward acceleration has to be caused by vertical gradient of the dynamic pressure. Figure 5d shows that F_L has in fact significantly positive values on the eastern side of the updraft. F_{NL} is also positive on the eastern side of the updraft (Figure 5e), but its magnitude is a factor of 1.5 smaller than that by F_L. Thus, the major cause to strengthen the updraft is due to F_L in accord with *Rotunno and Klemp* [1982]. As a whole, the updraft is intensified in its northeastern side (Figure 5a). For the 2.6 km-run, it is seen that the patterns of positive and negative regions for these terms are almost the same as in the 2.5 km-run, indicating that F_L is also the major contributor to the maintenance of the updraft in the right-mover. Comparing the intensity of F_L for the 2.5 km-run with that for the 2.6 km-run, however, the latter is clearly weaker.

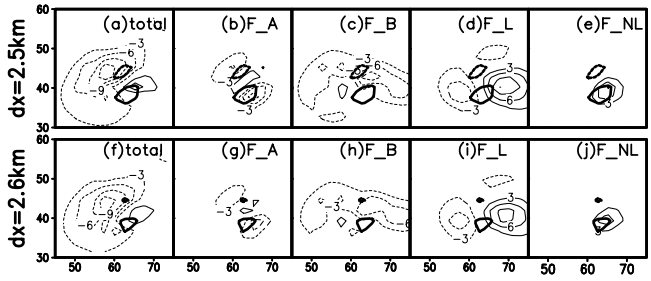

Figure 5. Horizontal distributions of the vertical velocity and the terms of the right-hand side of Equation (1) at z = 1 km at t = 40 min for the 2.5 km- (a–e), and 2.6 km-runs (f–j). Thin lines indicate (a) $F_A + F_B + F_L + F_{NL}$, (b) F_A, (c) F_B, (d) F_L, and (e) F_{NL} (contoured for every 3 $\times$ 10^{-3} m s^{-2}), and thick line the vertical velocity (contoured for every 2 m s^{-1}). The zero contoured lines are omitted. (f)–(j) are the same as (a)–(e) except for the 2.6 km-run.

[17] Figure 6 shows vertical cross sections of π_L, F_L, π_{NL} and F_{NL} along the centers of the updraft for the 2.5 km- and 2.6 km-runs. A comparison between linear and nonlinear terms (Figure 6b and 6d) shows that for both runs the linear terms are dominant over the nonlinear terms. The pressure minimum of π_L at around 4.5 km AGL for the 2.5 km-run is less than -90 Pa while that for the 2.6 km-run is only -80 Pa. It is also noted that the negative perturbation pressure extends more toward the ground for the 2.5 km-run than for the 2.6 km-run.

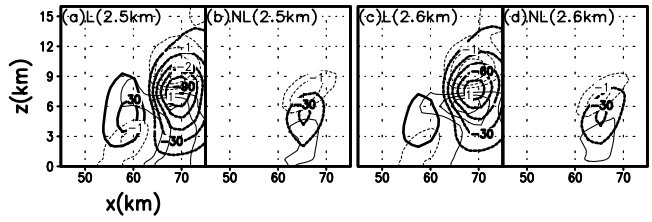

Figure 6. Vertical cross sections of π_L (thick contour line with every 15 Pa interval) and F_L (thin contour line with every 0.5 $\times$ 10^{-2} m s^{-2}) along y = 39 km at t = 40 min for the 2.5 km-run. (b) is the same as (a) except for π_{NL} and F_{NL}. (c) and (d) are the same as (a) and (b) except for the 2.6 km-run.

[18] Consequently, the upward upward pressure gradient force, PGF, is weaker for the 2.6 km-run, resulting in the weaker updraft. This, in turn, causes weaker generation of the vertical vorticity by the tilting and subsequent vertical stretching of the environmental horizontal vorticity (not shown).

[19] Equation (2) shows that the shear-induced perturbation pressure due to linear-interaction is proportional to the horizontal gradient of w, which depends linearly on w and a reciprocal of L. Thus, for a given value of w, the increase of L weakens the updraft by underestimating the shear-induced upward PGF. We have also examined other factors such as the change of the rain water mixing ratio and the surface temperature deficit which may possibly affect the storm behavior. Plots of these quantities similar to Figure 2 in fact show drastic changes between the 2.5 km- and 2.6 km-runs. However, these drastic changes appeared after t = 50–60 min, which is 10–20 min later than the drastic change appeared in the updraft. Thus, the rain fall and the surface temperature deficit do not seem to be the cause of the change in the storm behavior. The effects of numerical diffusion and subgrid turbulence could be other candidates for causing the drastic change in the behavior of the storm. However, unless one can think of some mechanism by which these diffusions operate selectively, it is difficult to explain the dissipation of the right-mover and the survival of the left-mover for the grid size larger than 2.6 km.

4. Conclusions

[20] Dependence of the numerically-simulated Del City supercell on horizontal grid size has been examined. It is found that there is a critical grid size above which the behavior of the simulated storm changes drastically. The initial storm splits into two at around t = 40 min and the right-side one evolves into a supercell when the grid size is less than 2.5 km. However, the split storm, which would be expected to become a right-mover, fails to develop into a supercell and dissipates eventually when the grid size is greater than 2.6 km. The principal reason for this failure results from the insufficient grid size to estimate properly the shear-induced dynamic pressure, which is important for maintaining the rotating updraft in a supercell [e.g., *Rotunno and Klemp* [1982]]. When the grid size is increased to 2.8 km, no long-lasting storm is observed any more.

[21] It is natural to expect that an increase in the grid size would cause a gradual quantitative change on a simulated storm such as weakening of the updraft intensity. However, the present study has demonstrated that only a small increase of the grid size by 100 m could change a qualitative behavior of the simulated storm drastically. This critical grid size is likely to vary from model to model and also to depend on storm type. For example, *Weisman et al.* [1997] suggests a much larger critical grid size of 4 km for a mid-latitude squall line for which a cold pool rather than the shear-induced dynamic pressure plays an important role. However, it is certain that any mesoscale model has a critical grid size above which the behavior of the convective storm changes drastically. If this is the case, one has to be careful in choosing the grid size when predicting convective storms or meso-β-scale precipitation system in which convective storms play an important role in maintaining the parent system.

[22] **Acknowledgments.** We would like to thank two anonymous reviewers for helpful suggestions and comments, which improved the manuscript greatly. The present work is partly supported by Grant-in-Aids for Scientific Research (B)(2) No. 15340154, the Ministry of Education, Culture, Sports, Science and Technology. This simulation was made using the Advanced Regional Prediction System(ARPS) developed by the Center for Analysis and Prediction of Storms (CAPS), University of Oklahoma. CAPS is supported by the National Science Foundation and the Federal Aviation Administration through combined grant ATM92-20009.

References

Adlerman, E. J., and K. K. Droegemeier, The sensitivity of numerically simulated cyclic mesocyclogenesis to variations in model physical and computational parameters, *Mon. Wea. Rev.*, *130*, 2671–2691, 2002.

Adlerman, E. J., K. K. Droegemeier, and R. P. Davies-Jones, A numerical simulation of cyclic mesocyclogenesis, *J. Atmos. Sci.*, *56*, 2045–2068, 1999.

Kato, T., Hydrostatic and non-hydrostatic simulations of the 6 August 1993 Kagoshima torrential rain, *J. Meteor. Soc. Japan*, *74*, 355–363, 1996.

Klemp, J. B., and R. B. Wilhelmson, The simulation of three-dimensional convective storm dynamics, *J. Atmos. Sci.*, *35*, 1070–1096, 1978.

Rotunno, R., and J. B. Klemp, The influence of the shear-induced pressure gradient on thunderstorm motion, *Mon. Wea. Rev.*, *110*, 136–151, 1982.

Weisman, M. L., W. C. Skamarock, and J. B. Klemp, The resolution dependence of explicitly modeled convective systems, *Mon. Wea. Rev.*, *125*, 527–548, 1997.

Xue, M., K. K. Droegemeier, V. Wong, A. Shapiro, and K. Brewster, *ARPS Version 4.0 User's Guide*, 380 pp., The Center for Analysis and Prediction of Storms, University of Oklahoma, 1995.

Yanase, W., H. Niino, and K. Saito, High-resolution numerical simulation of a polar low, *Geophys. Res. Lett.*, *29*, doi:10.1029/2002GL014736, 2002.

A. Noda and H. Niino, Ocean Research Institute, The University of Tokyo, 1-15-1, Minamidai, Nakano, Tokyo 164-8639, Japan. (noda@ori.u-tokyo.ac.jp)